HEALTH AND MEDICINE

Focusing light inside live tissue using reversibly switchable bacterial phytochrome as a genetically encoded photochromic guide star

Jiamiao Yang[1]*, Lei Li[1]*, Anton A. Shemetov[2]*, Sangjun Lee[3], Yuan Zhao[3], Yan Liu[1], Yuecheng Shen[1], Jingwei Li[1†], Yuki Oka[3], Vladislav V. Verkhusha[2‡], Lihong V. Wang[1‡]

Focusing light deep by engineering wavefronts toward guide stars inside scattering media has potential biomedical applications in imaging, manipulation, stimulation, and therapy. However, the lack of endogenous guide stars in biological tissue hinders its translations to in vivo applications. Here, we use a reversibly switchable bacterial phytochrome protein as a genetically encoded photochromic guide star (GePGS) in living tissue to tag photons at targeted locations, achieving light focusing inside the tissue by wavefront shaping. As bacterial phytochrome-based GePGS absorbs light differently upon far-red and near-infrared illumination, a large dynamic absorption contrast can be created to tag photons inside tissue. By modulating the GePGS at a distinctive frequency, we suppressed the competition between GePGS and tissue motions and formed tight foci inside mouse tumors in vivo and acute mouse brain tissue, thus improving light delivery efficiency and specificity. Spectral multiplexing of GePGS proteins with different colors is an attractive possibility.

INTRODUCTION

Optical technology has shown its increasing significance in biomedical research and modern medicine. Particularly, light focusing plays an important role in imaging with high resolution and sensitivity, and in precise optical energy deposition at targeted positions to achieve manipulation, stimulation, and therapy. However, microscopic refractive index inhomogeneity inherent to biological tissue scatters photons randomly and prevents light from focusing deep inside tissue. Consequently, conventional optical microscopy is fundamentally limited to superficial layers within approximately one optical transport mean free path from the tissue surface (~1 mm in biological tissue) (*1*). Recently, a rapidly developed technique—wavefront shaping—aims to overcome this limit and achieve a tight light focus deep inside tissue by creating constructive interference of scattered photons. On the basis of the methodologies to identify the optimal wavefront, wavefront shaping technologies fall into three categories: the feedback-based method (*2*, *3*), the transmission matrix method (*4*, *5*), and the optical phase conjugation (OPC) method (*6*–*10*). The OPC method, directly measuring the optimal wavefront of the tagged photons, provides the fastest focusing among all these methods and offers a solution for overcoming challenges associated with living tissue dynamics.

Focusing light inside scattering media with wavefront shaping requires a guide star at the target location, which provides feedback for finding the optimal incident optical field (*11*). Several types of guide stars have been developed, including ultrasonic (*12*–*14*), fluorescence (*15*, *16*), nonlinear optical (*17*, *18*), kinetic (*9*, *19*), photoacoustic (*2*, *20*), magnetic (*21*, *22*), and microbubble (*23*) mechanisms. To enable tissue type–specific in vivo applications, such as optogenetic control over targeted neurons, a genetically encoded guide star is desired. To our best knowledge, until now, no genetically encoded guide star has been demonstrated in wavefront shaping to focus light deep inside tissue in vivo. Thus, the wavefront shaping community still yearns for a genetically encoded guide star.

Here, we introduce a genetically encoded photochromic guide star (GePGS)—reversibly switchable bacterial phytochrome (RSBP)—into biological tissue to provide feedback for focusing light inside tissue (*24*). RSBP serves as an ideal genetically encoded guide star for in vivo applications due to the following characteristics: (i) RSBP works at the near-infrared (NIR) wavelength region, where photons are least attenuated by tissue, thus allowing maximum tissue penetration; (ii) RSBP can be genetically encoded and expressed inside targeted tissue in vivo, and their light-sensing chromophore, biliverdin, is abundant in mammalian tissue; and (iii) the absorption coefficient of RSBP can be rapidly and efficiently modulated (*25*) by both ballistic and scattered photons to induce local light field changes.

Using RSBP as a GePGS, we developed a digital OPC (DOPC) system to achieve light focusing inside mammalian tissue in vivo. By modulating the optical absorption of RSBP at 20 Hz, we successfully tagged photons passing through GePGS with high specificity and efficiency. Tagging with lock-in detection fights against fast tissue motion, such as blood flow and respiration motion. We experimentally demonstrated a focus of 25 μm diameter inside scattering media. Furthermore, we successfully focused light on the targeted tumors in mice in vivo and on live neurons in acute brain tissue. The combination of our proposed GePGS and wavefront shaping technology opens up a new avenue for focusing light deep inside tissue in vivo, which holds potential for broad biomedical applications, such as deep-tissue photothermal therapy of tumors and optogenetic control of targeted neurons in the deep brain.

[1]Caltech Optical Imaging Laboratory, Andrew and Peggy Cherng Department of Medical Engineering, Department of Electrical Engineering, California Institute of Technology, Pasadena, CA 91125, USA. [2]Department of Anatomy and Structural Biology, and Gruss Lipper Biophotonics Center, Albert Einstein College of Medicine, Bronx, NY 10461, USA. [3]Division of Biology and Biological Engineering, California Institute of Technology, Pasadena, CA 91125, USA.
*These authors contributed equally to this work.
†Present address: Centre for Optical and Electromagnetic Research, Chinese National Engineering Research Center for Optical Instruments, Zhejiang University, Hangzhou 310058, China.
‡Corresponding author. Email: vladislav.verkhusha@einstein.yu.edu (V.V.V.); lvw@caltech.edu (L.V.W.)

RESULTS

Principle of GePGS-guided optical focusing inside scattering media

Figure 1 depicts the principle of GePGS-guided optical focusing inside scattering media. The GePGS used here is a photosensory core module (PCM; 55 kDa) of RSBP from *Deinococcus radiodurans* bacteria, termed DrBphP-PCM (see Materials and Methods). The structure and properties of DrBphP-PCM's chromophore, a covalently attached biliverdin IXα (BV) (*26*, *27*), are shown in Fig. 1A. BV photoisomerization leads to two absorbing states, one of which absorbs at 670 to 700 nm (the Pr state, termed "OFF" state) and the other absorbs at 740 to 780 nm (the Pfr state, termed "ON" state). DrBphP-PCM exhibits natural photochromic behavior: When illuminated by 630- to 690-nm light, DrBphP-PCM is photoswitched from the Pr state to the Pfr state; when illuminated by 730- to 790-nm light, DrBphP-PCM is photoswitched from the Pfr state to the Pr state. The molar absorption spectra of oxyhemoglobin (HbO_2) and deoxyhemoglobin (Hb) and the two states of DrBphP-PCM are shown in Fig. 1B. DrBphP-PCM has obvious changes in terms of spectral absorption characteristics between its two states. The absorption coefficient ratio (black solid line in Fig. 1B) between its two states (Pfr/Pr) is ~10 at 780 nm, which is selected as the working wavelength for the GePGS-guided DOPC system. DrBphP-PCM also has some, albeit weak, intrinsic fluorescence in the Pr state (*28*), which can be used to quickly verify its successful expression in tissue. Both absorption and fluorescence of DrBphP-PCM can be reversibly photoswitched (fig. S1).

Figure 1C shows the time sequence of the GePGS-guided DOPC system. Figure 1 (D to F) and movie S1 show the corresponding operations for focusing light inside a scattering medium. The GePGS is illuminated by 637- and 780-nm light alternatingly to switch it on and off at a frequency f_{mod} of 20 Hz for N cycles. Consequently, the frequency of the 780-nm photons passing through the GePGS is shifted to $f_0 \pm nf_{mod}$, where f_0 is the original frequency of the 780-nm light, and n = 1,2,3, … (note S1). To obtain the wavefront of the tagged photons with frequencies of $f_0 \pm f_{mod}$, a reference beam with a frequency of f_0 is introduced to interfere with the photons passing through the scattering medium (Fig. 1E). In each cycle, the GePGS is switched to the ON state by 637-nm light illumination for 24 ms (Fig. 1D), and then, it is gradually switched off by 780-nm light illumination for 26 ms (Fig. 1E). Two holograms with a time interval of $1/(2f_{mod})$ are recorded during the switching off process. Then, the wavefront of the tracked photons is calculated from the recorded holograms (see Materials and Methods). Last, a digital micromirror device (DMD) is used to modulate the reference beam to produce a conjugate wavefront of the tracked photons, which focused onto the

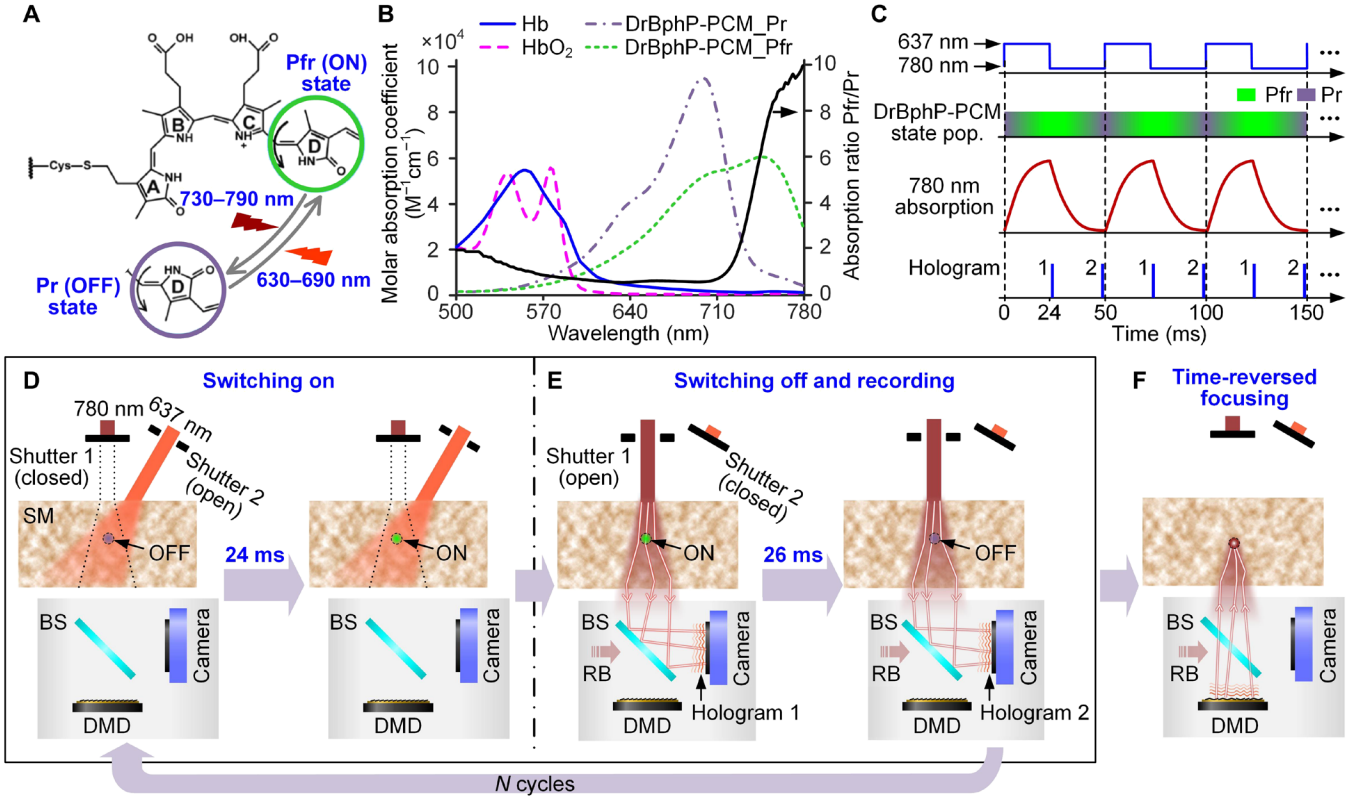

Fig. 1. Principle of GePGS-guided optical focusing inside scattering media. (**A**) Photoswitching of DrBphP-PCM chromophore from the Pfr state to the Pr state, and vice versa, induced by 780- and 637-nm light illumination, respectively. The photoswitchings result from the out-of-plane rotation (black arrows) of the D ring of biliverdin about the adjacent C15/16 double bond between the C and D pyrrole rings. (**B**) Molar absorption spectra of oxyhemoglobin (HbO_2), deoxyhemoglobin (Hb), Pfr (ON), and Pr (OFF) states of DrBphP-PCM. The absorption coefficient ratio (black solid line) between the two states (Pfr/Pr) is ~10 at 780 nm. (**C**) Time sequence of GePGS-guided DOPC system (pop., population). (**D**) Switching the DrBphP-PCM to the ON state by a 637-nm laser beam with a duration of 24 ms. (**E**) Switching the DrBphP-PCM to the OFF state by a 780-nm laser beam with a duration of 26 ms and capturing two holograms with an interval of 25 ms. (**F**) Time-reversed focusing on the GePGS inside a scattering medium. BS, beam splitter; RB, reference beam.

GePGS, as shown in Fig. 1F (note S2 and fig. S2). To minimize the effect of fast motions in scattering media, we average each hologram over *N* cycles (note S3).

Experimental setup and characterization

DrBphP-PCM–based GePGS was injected at a targeted location inside a scattering medium. Its absorption state was controlled by the illumination of 780- or 637-nm light. A DMD-based DOPC system was built to realize optical focusing inside a scattering medium with the guidance of the GePGS, as illustrated in Fig. 2A (see Materials and Methods, note S4, and figs. S2 and S3). As shown in Fig. 2B, an observation setup was introduced to characterize the GePGS-guided optical focusing inside scattering media. DrBphP-PCM (~300 μM concentration) was injected in the central hole of a sample holder placed between two scattering media (DG-120, Thorlabs). The time-reversed beam was partially split by a beam splitter (BS2) into the verification camera, located on the conjugate plane of the GePGS, to observe the light focus. Sample holders with different hole diameters were used to control the size of the GePGS. Figure 2C shows that the diameters of GePGS-guided foci matched the corresponding sizes of the GePGS (top row). In the control experiments where 637-nm illumination was blocked, no light focus was formed (bottom row). We have experimentally demonstrated GePGS-guided focus inside scattering media with a diameter down to 25 μm. The peak-to-background ratios (PBRs) of each focus were computed to quantify their focusing contrasts, as shown in Fig. 2D. Theoretically, the PBR is inversely proportional to the area of the guide star (*14*, *29*–*31*). However, the PBR reached the maximum when the diameter of the GePGS was 50 μm instead of 25 μm. The signal-to-noise ratio (SNR) of the averaged differential hologram (note S5) decreased as the diameter of the GePGS decreased (red dashed line in Fig. 2D), which limited the experimental PBR of the time-reversed focus.

Tissue-mimicking phantom experiments

To demonstrate GePGS-guided light focusing inside a tissue-mimicking phantom, we injected a solution of purified DrBphP-PCM into a square tube, which was sandwiched by two 1.5-mm-thick intralipid-gelatin phantoms (see Materials and Methods), as shown in Fig. 3A. The concentration of the GePGS was 300 μM, and the reduced scattering coefficient of the intralipid-gelatin phantoms was ~10 cm^{-1}. Figure 3B shows the normalized transmittance of the 780-nm light passing through square tubes with different inner dimensions during switching off. The measured light transmittance in the OFF state was 70, 81, 89, and 95%, when the inner dimensions of the square tubes were 300, 200, 100, and 50 μm, respectively. Figure 3C shows the time-reversed focusing on the tubes. The PBRs reached 38.2, 23.9, 10.4, and 5.3 for the inner dimensions of 50, 100, 200, and 300 μm, respectively. To verify that light only focuses on the GePGS, instead of other places, we sandwiched two tubes (length of the inner side, 50 μm) side by side, filled with a solution of purified DrBphP-PCM and bovine blood, respectively, between the two intralipid-gelatin phantoms. The time-reversed light pattern was shown in Fig. 3D, where the white dot-dashed lines illustrate the position of the tube filled with blood. Figure 3E is the normalized intensity distribution along the yellow dashed line in Fig. 3D. It is obvious that light was focused only on the GePGS, not on the blood.

To show the advantage of the developed GePGS in live mammals, we established a U87 cell line stably expressing DrBphP-PCM and then demonstrated the time-reversed focusing. A tube (length of the inner side, 300 μm), sandwiched between the two intralipid-gelatin

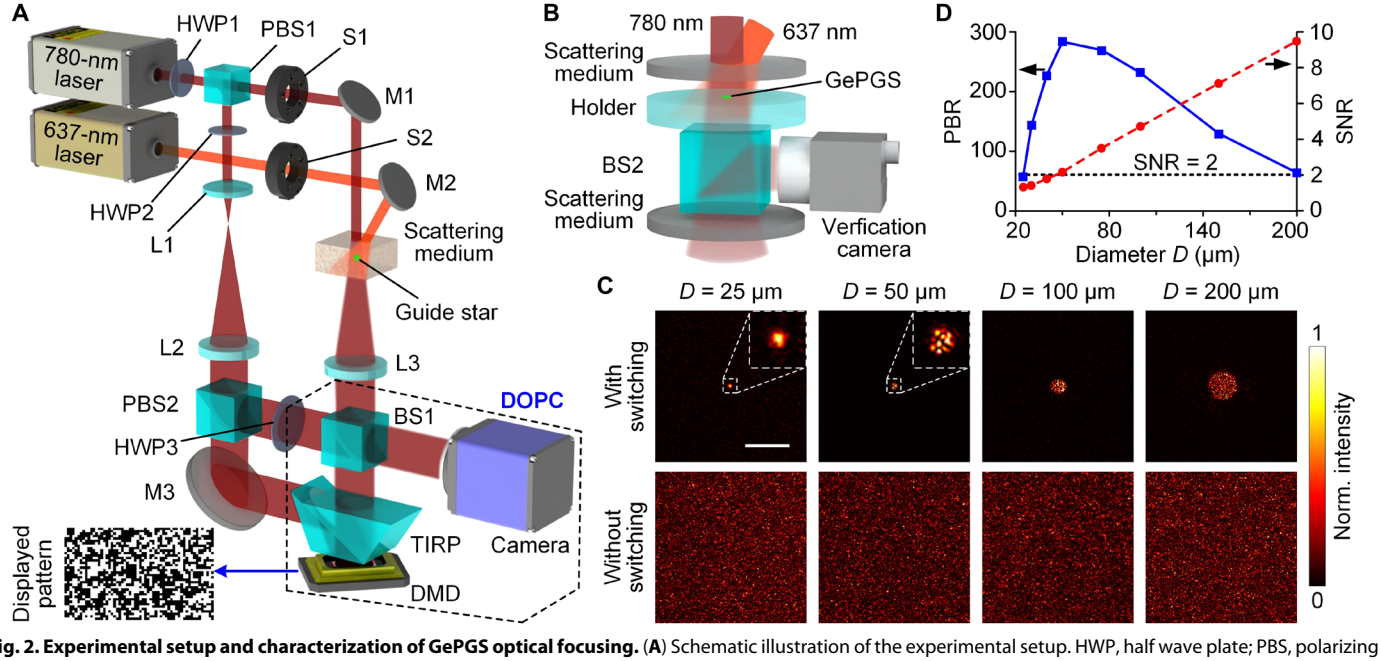

Fig. 2. Experimental setup and characterization of GePGS optical focusing. (**A**) Schematic illustration of the experimental setup. HWP, half wave plate; PBS, polarizing beam splitter; S, shutter; M, mirror; L, lens; BS, beam splitter; TIRP, total internal reflection prism; DMD, digital micromirror device. (**B**) Setup for quantifying the GePGS-guided focusing inside a scattering medium. (**C**) Normalized (Norm.) intensity distributions of the optical foci in between two scattering media with different diameters (*D*) of guide stars. Top row, with 637-nm light switching; bottom row, without 637-nm light switching. Each image is self-normalized. Scale bar, 300 μm. (**D**) PBRs of the foci with different GePGS diameters, and the corresponding SNRs of the captured holograms.

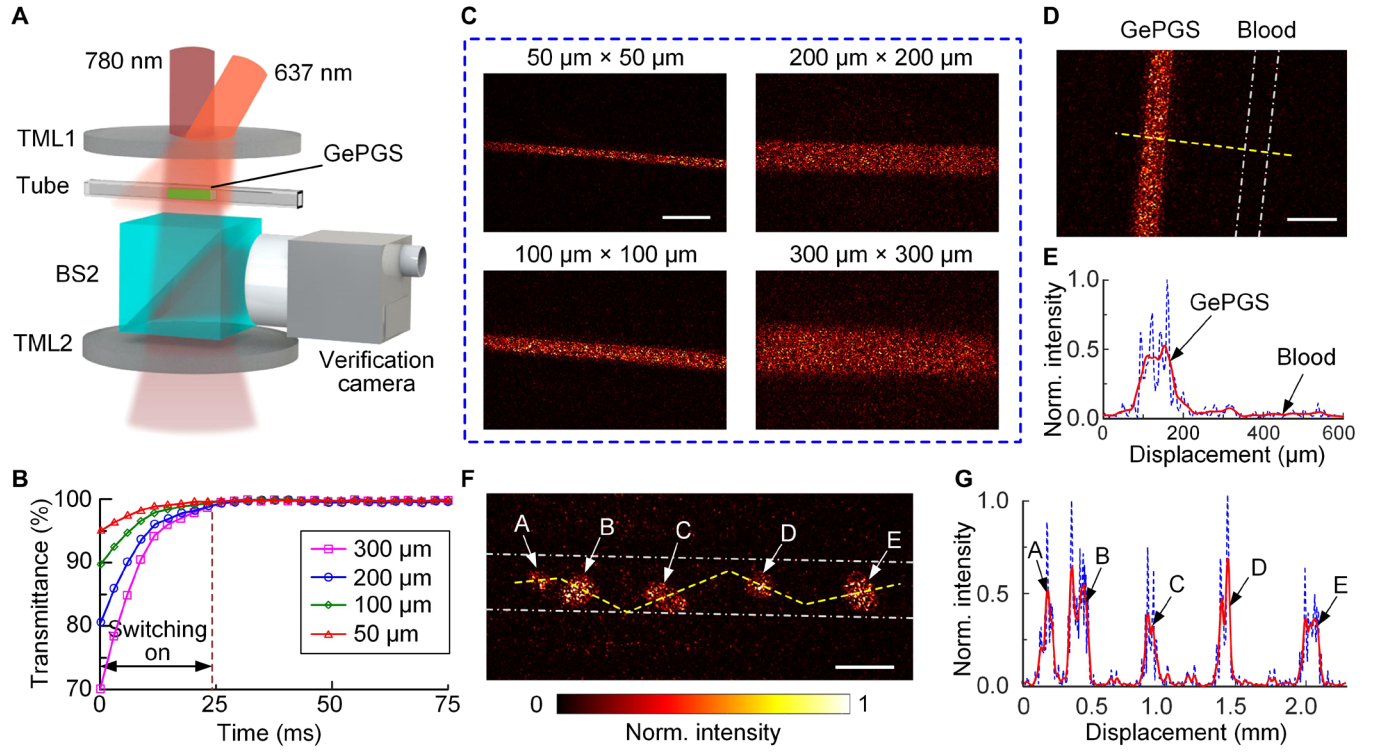

Fig. 3. In vitro demonstration of focusing light onto GePGS inside scattering media. (**A**) Experimental setup for in vitro demonstration. TML, tissue-mimicking layer. (**B**) Normalized transmittance of the light passing through the tubes with different diameters filled with GePGS (300 μM). The inner dimensions of the square tubes were 50, 100, 200, and 300 μm. (**C**) Images of the focused light onto GePGS injected into the tubes with different sizes. Scale bar, 300 μm. (**D**) Image shows that light is focused only onto the GePGS, not blood. Two tubes filled with GePGS and blood are placed side by side. The white dash-dotted lines represent the inner walls of the tube filled with blood. The inner dimensions of the tubes were both 100 μm. Scale bar, 200 μm. (**E**) Normalized intensity distribution along the yellow dashed line in (D). The blue dashed line is the measured value, and the red solid line is the smoothed curve with a span of 10 points. (**F**) Image of the focused light onto a tube filled with U87 cells expressing GePGS. It shows that light is focused onto the GePGS-expressing cells/cell clusters. The white dash-dotted lines represent the inner walls of the tube. Scale bar, 300 μm. (**G**) Normalized intensity distribution along the yellow dashed line in (F). The blue dashed line is the measured value, and the red solid line is the smoothed curve with a span of 10 points.

phantoms, was filled with GePGS-expressing U87 cells. Figure 3F shows the time-reversed light pattern, where the white dot-dashed lines represent the inner wall of the tube. It is clear that the time-reversed light focused on the GePGS-expressing cells or cell clusters. Figure 3G illustrates the normalized intensity distribution along the yellow dashed line in Fig. 3F, and five cells or cell clusters in the field of view with different sizes were identified.

Focusing inside mouse tumors in vivo

Next, we demonstrated GePGS-guide focusing inside murine tissue in vivo. The experimental setup is shown in Fig. 4A. The U87 cells expressing GePGS were injected to a mouse ear to induce tumors. We conducted the DOPC experiment on the mouse 5 days after injection. The mouse ear was illuminated by 637- and 780-nm light alternatingly with a modulation frequency of 20 Hz. The DOPC system was used to record the wavefront of the 780-nm scattered light and play back the reference beam with an optimal wavefront to focus light on the tumor inside the mouse ear. In the mouse ear, both the GePGS and the fast decorrelation components, such as blood flow and respiratory motion, tagged photons in the process of OPC (Fig. 4B). This inevitably led to a competition between the fast decorrelation components and the GePGS in terms of light focusing (*10*). Here, the frequency lock-in technology used in the modulation of the GePGS substantially suppressed the impact of the fast decorrelation components. Thus, we can specifically filter out the photons tagged by the GePGS only and reject the other unwanted photons (note S6 and fig. S4).

To achieve a high contrast focus on the tumor inside the mouse ear, we modulated the GePGS for *N* cycles. Because the tumor was close to the right side of the mouse ear, a microscope was placed on the same side of the mouse ear to observe photons transmitted through the ear from the left side (Fig. 4A). Figure 4B shows the speckle correlation coefficient as a function of time for the mouse ear. The time-reversed foci, with different *N*, on the tumor were captured by the microscope (Fig. 4C, left three panels). In the control experiment, where the light modulation was off, no light focus was observed (Fig. 4C, right). The detected signals of tagged photons (at 20 Hz) increase with increasing *N* (Fig. 4D, red circle dashed curve). The PBR of the time-reversed focus also increases with *N* but reaches a maximum when averaged over 115 cycles and starts to decrease if averaged more (Fig. 4D, blue squared solid curve, and movie S2). This trend is because slow decorrelation (Fig. 4B) becomes obvious as the overall time of DOPC increases. With the capability of selective delivery of light on to the specific tissue types, such as tumors, the GePGS-guided wavefront shaping advances light-driven therapy of targeted tumors at depths in vivo.

Focusing inside the acute brain tissue

Focusing light inside the brain can directly benefit neuroscience research, which, however, remains largely unexploited. Because of the

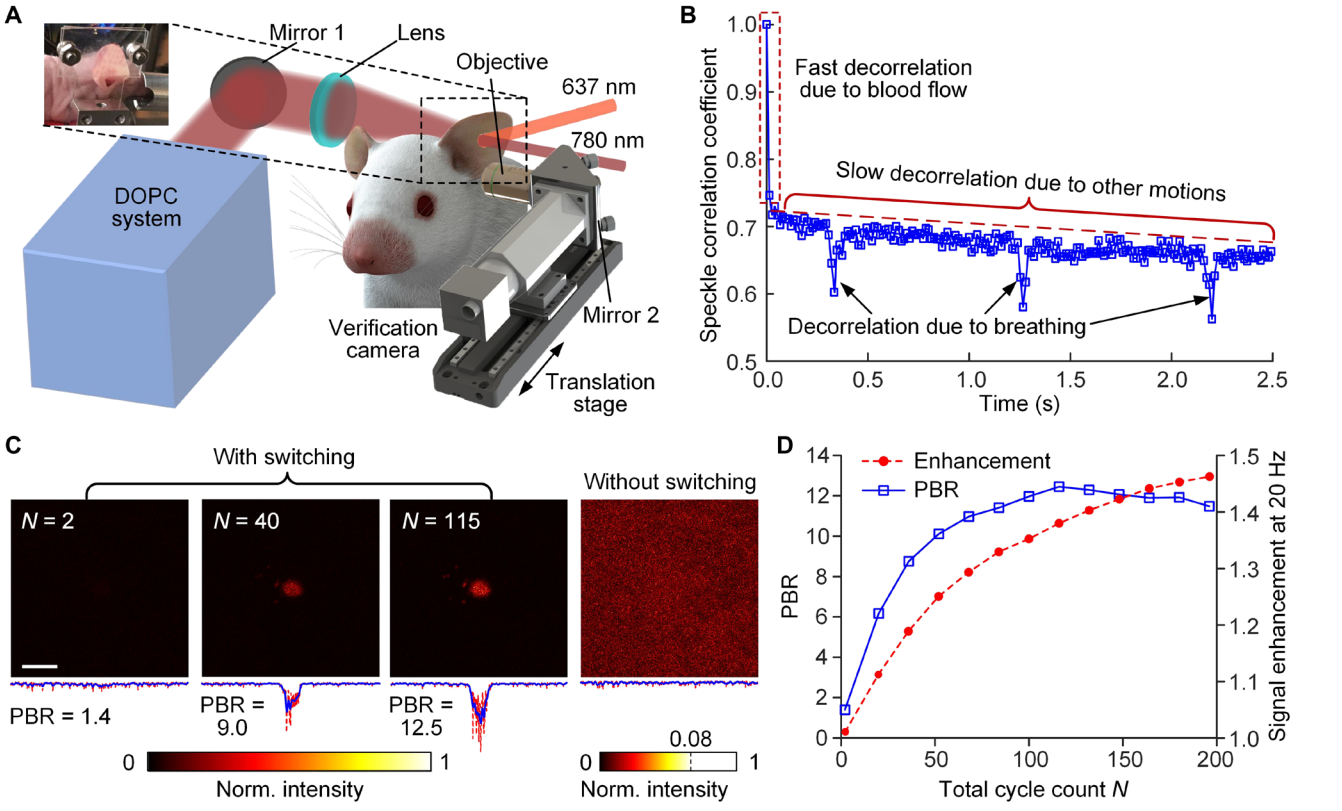

Fig. 4. In vivo demonstration of focusing light inside tumors. (**A**) Schematic of the setup for focusing light inside tumors on the mouse ear in vivo. A microscope is placed on a translation stage and can be moved horizontally into the light path to image the time-reversed focus. (**B**) Speckle correlation coefficient as a function of time for a living mouse ear. Three speckle decorrelation characteristics were identified. (**C**) Normalized intensity distributions of the optical foci inside the tumor on the mouse ear. Left, with 637-nm light switching for $N = 2$, 40, and 115 cycles; right, without 637-nm light switching. Scale bar, 100 μm. (**D**) Signal enhancement of tagged photons (at 20 Hz) and the PBR of time-reversed focusing as a function of the total cycle count N.

strong optical scattering nature of the brain, current light delivery for optogenetic manipulations and optical readouts still primarily uses invasive optical fiber implants to reach targets in the deep brain. To determine whether DrBphP-PCM works in neurons, we first transduced with adeno-associated viruses (AAVs) encoding DrBphP-PCM in primary cultured neurons. Four days after the AAV infection, intrinsic NIR fluorescence of DrBphP-PCM that was evenly distributed inside the cells was detected, which confirmed a successful transduction (fig. S5). Next, we transduced the mouse brain with AAVs in vivo. Fluorescence images showed a successful expression of DrBphP-PCM in the brain (Fig. 5A, left), although the imaging resolution was not very high due to the strong optical scattering of brain tissue. To demonstrate light focusing inside the live brain tissue, we harvested a 900-μm-thick brain slice (see Materials and Methods). On this brain slice, the DrBphP-PCM was expressed close to the bottom side (Fig. 5A, right panel view from the bottom side of the brain slice). The DOPC experimental setup is shown in Fig. 5B. In the brain slice, the principal decorrelation is slow decorrelation with a decorrelation time of 8.7 s (Fig. 5C). After modulating the GePGS for 20 cycles, the tagged photon signals at 20 Hz increased by a factor of ~2 (Fig. 5D). An optical objective lens was placed on the bottom side of the brain slice to observe the light focus (Fig. 5B, inset). With 20 cycles of modulation, we observed a time-reversed focus on the brain slice with a PBR of 19.8 (Fig. 5E, left), which matches well with the fluorescence image (Fig. 5A, right). In the control experiment, without light modulation, no light focus was observed (Fig. 5E, right). The tagged photon signals increased with increasing N (Fig. 5F, red circle dashed curve). The PBR of the time-reversed focus also increased with N but reached the maximum at N of 20 and then started to decrease thereafter (Fig. 5E, blue squared solid curve, and fig. S6), because the dominant slow decorrelation caused a mismatch between the recorded wavefront and the optimal wavefront during the time of wavefront playback.

DISCUSSION

We have introduced an RSBP, such as DrBphP-PCM, as a GePGS and experimentally demonstrated time-reversed optical focusing inside scattering media. The RSBP, working in the NIR window, maximizes the optical penetration in biological tissue. The optical absorption of the RSBP is controllable upon light illumination. Moreover, the RSBP is genetically encoded and expressed inside tissue through either exogenous cell translation or native expression via virus infection. In addition, because this guide star is reversibly switchable, we can use the lock-in technique to reduce the unwanted background and boost the signal. Inside live tissue, blood flow and respiratory motion, inducing fast speckle decorrelation, can also tag photons and thus reduce the modulation depth from the guide stars. To fight against the fast decorrelation in vivo, we modulated the absorption of the GePGS at 20 Hz. By detecting the light field at the lock-in frequency of 20 Hz, the influence of the fast decorrelation components was minimized, and the time-reversed light was specifically

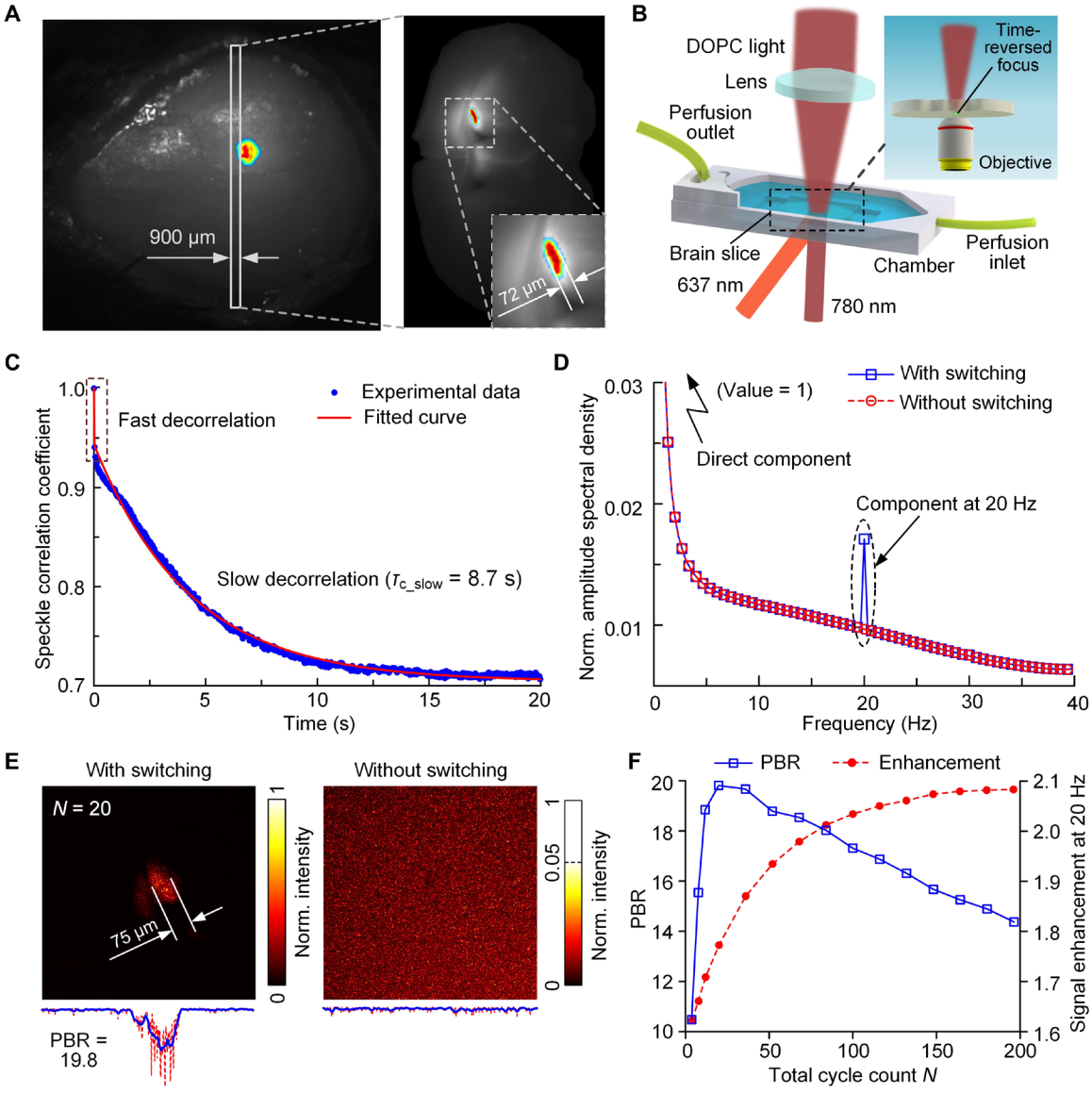

Fig. 5. Demonstration of focusing light inside brain slices. (**A**) Fluorescence images of the transduced mouse brain in vivo, and a live brain slice showing expression of the GePGS. The differential fluorescence signals between the ON and OFF states highlight the brain tissue expressing RSBPs, which are shown in color, and the background signals are shown in gray. Excitation wavelength, 630 nm. (**B**) Schematic of the setup for focusing light inside brain slices. (**C**) Speckle correlation coefficient as a function of time for a live brain slice. Two speckle decorrelation characteristics are identified. (**D**) Normalized amplitude spectral density of the detected photons, where a peak is observed at 20 Hz with light switching. (**E**) Normalized intensity distributions of the optical foci inside a brain slice. Left, with 637-nm light switching for N = 20; right, without 637-nm light switching. (**F**) Signal enhancement of tagged photons (at 20 Hz) and the PBR of time-reversed focusing as a function of the total cycle count N.

focused onto the GePGS-expressing tumor in vivo. Taking advantage of both the tissue-specific expression and effective light modulation of the GePGS, light can be effectively focused onto targeted tissue, such as tumors, at depth, which promises new applications such as advanced photodynamic therapy (PDT). Conventionally, PDT uses NIR light to activate photosensitizers for tumor destruction (*32*, *33*). However, the strong tissue scattering substantially reduces the light delivery efficiency and limits the penetration of PDT. Now, the GePGS-guided light focusing overcomes the limitations and may facilitate PDT with effective photon utilization at previously unreachable tissue depths.

Noninvasively focusing light deep inside living tissue promises many biomedical studies, especially for neuroscience, where light is routinely used for both monitoring neural activity with genetically encoded voltage or calcium indicators (*34*, *35*) and controlling neural activity via optogenetic actuators (*36*, *37*). Although advanced optical imaging techniques, such as multiphoton microscopy, adaptive optical microscopy, and photoacoustic tomography have substantially extended the depths of optical access in vivo (*17*, *38*, *39*), noninvasive light focusing in the diffusive regime in living brain tissue remains challenging. We successfully expressed GePGS in neurons using viral transduction. After multiple cycle modulation of the GePGS, scattered photons have been effectively tagged and an optical focus has been created inside the live brain tissue. Because genetic encoding can target selected cell populations, GePGS and light-sensitive neural activity actuators can be coexpressed in the same neurons; then, light

can be focused onto the targeted neurons to induce neural stimulations. RSBP-based GePGS itself can be the optogenetic actuators (*40*). Thus, the GePGS-guided photons can specifically trigger the targeted cells, without blind activation of background neurons. In addition, different cell populations can potentially be targeted spectrally. In other words, GePGS proteins of different colors can be addressed by selecting the matched switching optical wavelengths. Therefore, GePGS-guided optical focusing not only substantially increases the light delivery efficiency and the specificity of noninvasive deep-brain manipulations but also enables multiplex neural control.

Although the GePGS has been demonstrated on the basis of the OPC-based wavefront shaping method, the guide star itself and the frequency modulation method are also compatible with the feedback-based wavefront shaping method. The amplitude and phase contribution of each incident field component can be optimized based on the feedback signal from the GePGS at the modulation frequency. The physical limit of the photoswitching time for DrBphP-PCM, the GePGS used in this work, is 1 ms (*25*), which allows further acceleration of our DOPC response to fight against tissue optical decorrelation and thus permits even deeper light focusing. Moreover, the combination of GePGS-guided focusing and photoacoustic tomography, which provides high spatial resolution imaging in deep tissue based on optical contrast (*39*), is another appealing direction to explore. Photoacoustic tomography can directly visualize the light focus in deep tissue and image the focused light-induced biological activities, such as neuron firing and metabolic responses of tumors.

MATERIALS AND METHODS

Plasmid construction

The *DrBphP* gene was provided by J. Ihalainen (University of Jyväskylä, Finland). For mammalian expression, the PCM part encodings of the first 502 amino acids of the *DrBphP* gene were polymerase chain reaction (PCR)–amplified as a Nhe I–Not I fragment and cloned into the pEGFP-N1 plasmid instead of enhanced green fluorescent protein (EGFP) (Takara/Clontech). For bacterial expression, the PCM encoding part of the *DrBphP* gene was PCR-amplified as a Bgl II–Hind III fragment and cloned into a pBAD/HisB vector (Life Technologies/Invitrogen). For virus production, the PCM encoding part of the *DrBphP* gene was PCR-amplified as a Nhe I–Eco RI fragment and cloned into a pAAV-CW3SL-EGFP plasmid under control of CAMKII promoter instead of EGFP (Addgene, no. 61463). Resulted plasmid was called pAAV-CAMKII-DrPCM.

Protein expression and characterization

LMG194 host cells (Life Technologies/Invitrogen) were used for protein expression. A pWA23h plasmid encoding heme oxygenase (HO) from *Bradyrhizobium ORS278* (*hmuO*) under the rhamnose promoter was cotransformed with a pBAD/HisB plasmid encoding DrBphP-PCM with a polyhistidine tag. The bacterial cells were grown in restricted medium (RM) supplemented with ampicillin, kanamycin, and 0.02% rhamnose at 37°C for 6 to 8 hours, followed by induction of protein expression by adding 0.002% arabinose and incubation for 24 hours at 18°C. The protein was purified with Ni-NTA agarose (Qiagen). The sample was desalted using PD-10 columns (GE Healthcare). Absorption spectra of DrBphP-PCM, dissolved in phosphate-buffered saline, were measured using a standard spectrophotometer (Hitachi U-2000) with a 100-μl quartz microcuvette (Starna Cells). The spectrum of the Pr state (OFF state) DrBphP-PCM was measured without a photoswitching light source because the OFF state was the ground state. To measure the ON state spectra, we carried out photoswitching with a 636/20-nm custom-assembled light-emitting diode (LED) source placed above the microcuvette. The photoswitching beam direction was orthogonal to the optical beam path of the spectrophotometer. The ON state spectra were measured after the photoswitching was completed, and the LED was turned off to avoid interference with the measurement. Because of the extremely low light intensity (<1 $\mu W\ cm^{-2}$), changes in the absorption spectra of DrBphP-PCM induced by the light illumination inside the spectrophotometer were negligible.

Mammalian cell culture

U87 cells (American Type Culture Collection, catalog no. HTB-14) were grown in Dulbecco's modified Eagle's medium supplemented with 10% fetal bovine serum, a penicillin-streptomycin mixture, and 2 mM glutamine (all from Invitrogen/Life Technologies) at 37°C in 5% CO_2 air atmosphere. We obtained a U87 stable preclonal mixture by transfecting cells with the pDrBphP-PCM-IRES2-mCherry plasmid. Plasmid transfection was performed using Effectene (Qiagen). Cells were further selected with hygromycin B (75 $\mu g\ ml^{-1}$) (Gold Biotechnology) and enriched using a FACSAria sorter (BD Biosciences) equipped with a 561-nm laser and a 610/20-nm emission filter. For further culturing of U87 cells stably expressing DrBphP-PCM, the medium was supplemented with hygromycin B (75 $\mu g\ ml^{-1}$).

Large-scale preparation of AAVs

High-titer AAV particles were obtained as described (*41*). Briefly, plasmid DNA for AAV production was purified with a NucleoBond Xtra Maxi EF kit (Macherey-Nagel). Human embryonic kidney (HEK) 293FT (Thermo Fisher Scientific, no. R70007) cells were cotransfected with AAV genome plasmid pAAV-CAMKII-DrPCM, AVV9 capsid plasmid pAAV-PHP.eB (provided by V. Gradinaru, California Institute of Technology), and pHelper (Cell Biolabs) using polyethyleneimine (Santa Cruz Biotechnology). Cell media were collected 72 hours after transfection. 120 hours after transfection, cells and media were collected and combined with media collected at 72 hours. Cells were harvested by centrifugation and then lysed with salt active nuclease (SAN; ArcticZymes). Polyethylene glycol (PEG) (8%) was added to media, incubated for 2 hours on ice, and then pelleted. PEG pellet was treated with SAN and combined with lysed cells. Cell suspension was clarified by centrifugation. Supernatant was applied on iodixanol gradient and subjected to ultracentrifugation for 2 hours and 25 min at 350,000*g*. Virus fraction was collected, washed, and enriched on an Amicon 15 centrifuge device with molecular weight cutoff of 100 kDa. Purified virus was stored at 4°C. Virus titer was defined by quantitative PCR (qPCR). Aliquot of virus was consequently treated with deoxyribonuclease I and proteinase K and then used as a template for qPCR. Nhe I–digested pAAV-CAMKII-DrPCM plasmid with known concentration was used as a reference.

Primary cultured neuron imaging

Murine hippocampal primary neurons were cultured in Neurobasal medium supplemented with B27 (both Thermo Fisher Scientific). Neurons were transduced with 10^{10} viral genomes (vg) per well in a 24-well plate on day 10 in vitro and imaged with an Olympus IX81 inverted epifluorescence microscope on day 14 in vitro. The microscope was equipped with a 100-mW 617-nm LED source (Mightex), a 20× 0.45 numerical aperture air objective lens (UPlanSApo, Olympus), and an ORCA-Flash4.0 camera (Hamamatsu).

Details of the experimental setup

We built a DMD-based DOPC system, sketched in Fig. 2A, to focus light inside scattering media with the guidance of the GePGS. Two collimated light beams with wavelengths of 780 nm (MBR-100, Coherent Inc.) and 637 nm (12V-TTL-637nm-2W, Laserland Inc.) were generated by two continuous-wave laser sources. The 780-nm light beam was subsequently split into a reference beam and a sample beam by a variable ratio beam splitter, which was composed of a half-wave plate (HWP1) and a polarizing beam splitter (PBS1). The 780-nm sample beam and the 637-nm switching beam were reflected by mirrors M1 and M2, respectively, to illuminate the scattering medium. Shutters S1 and S2 were used to control the two beams to switch the absorption of the GePGS at a frequency of 20 Hz. A lens L3 with a focal length of 40 mm collected the 780-nm photons passing through the scattering medium. The 780-nm reference beam was expanded by a lens pair (L1 and L2) and then split into two beams by another variable ratio beam splitter (HWP2 and PBS2). The reflected beam was combined with the 780-nm beam from the scattering medium through a beam splitter (BS1), and their interference pattern was captured with an sCMOS (scientific complementary metal–oxide semiconductor) camera (PCO.edge 5.5, PCO). In each illumination cycle, two holograms, $I_{inter1}(x, y)$ and $I_{inter2}(x, y)$, were captured with a time interval of 25 ms during the GePGS switching off process (Fig. 1E). We averaged each hologram over N cycles, resulting in the averages $\bar{I}_{inter1}(x,y)$ and $\bar{I}_{inter2}(x,y)$. The beam transmitted through PBS2 was reflected by a mirror (M3) and a total internal reflection prism (TIRP) and then illuminated on a DMD (SuperSpeed V-9501, Texas Instruments Inc., 1920 × 1080 pixels) with a special incident angle (10°). The curvature of the DMD was compensated for to reduce displayed wavefront error (note S4 and fig. S3A). The DMD and the camera were placed conjugated relative to BS1, and mapping between the camera pixels and DMD pixels was measured (note S4 and fig. S3B). By displaying the following binary amplitude map $D_{DMD}(x, y)$ (note S2 and fig. S2), the DMD modulated the reference beam to form a phase-conjugated focus inside the scattering medium

$$D_{DMD}(x,y) = \begin{cases} 1, & \bar{I}_{inter1}(x,y) \geq \bar{I}_{inter2}(x,y) \\ 0, & \bar{I}_{inter1}(x,y) < \bar{I}_{inter2}(x,y) \end{cases} \quad (1)$$

Intralipid-gelatin phantom preparation

The intralipid-gelatin phantom was made from intralipid (Intralipid 20%, Fresenius Kabi, Sweden), porcine skin gelatin (10% by weight, G2500-1kG, Sigma-Aldrich, USA), and deionized water (*42*). With a lipid concentration of 1.5 g ml^{-1}, the reduced scattering coefficient μ_s' was ~10 cm^{-1}. Acrylic spacers with a thickness of 0.15 cm were sandwiched between two acrylic sheets to accurately control the thickness of the intralipid-gelatin phantom to be 0.15 cm (equivalent to 1.5 l_t', where l_t' denotes the transport mean free path).

Preparation of animals

Adult 2- to 3-month-old female nude mice (Hsd:Athymic Nude-FoxlNU, Harlan; body weight: ~20 to 30 g) were used for all in vivo experiments. All experimental procedures were carried out in conformity with laboratory animal protocols approved by the Institutional Animal Care and Use Committee at California Institute of Technology (Wang lab 1737). Throughout the experiment, the mouse was maintained under anesthesia with 1.5% vaporized isoflurane. The anesthetized mouse was taped to a laboratory-made animal holder. To implant xenograft tumors into the mice, ~10^6 U87 cells, stably expressing DrBphP-PCM, in 0.05 ml of PBS were injected into a mouse ear with the guidance of a stereomicroscope (A60 F, Leica).

Measurement of the speckle correlation time of live tissue

To measure the speckle correlation coefficient of live tissue, the camera in the DOPC system worked with a region of interest of 400 × 200 pixels and a frame rate of 200 Hz. The speckle correlation coefficient at time t_m was calculated as the correlation between two speckle images captured at $t = 0$ and $t = t_m$ (*43*). By fitting the speckle correlation coefficients with the function of $\alpha_{cor} = A \exp(-2t/\tau_c) + B$, where A and B are constants, the decorrelation time τ_c can be obtained, which corresponds to the speckle correlation coefficient that decreased to $1/e^2 + B$.

DrBphP-PCM expression in the mouse brain in vivo

All procedures followed the animal care guidelines from the National Institutes of Health for the care and use of laboratory animals, and were approved by the Institutional Animal Care and Use Committee at California Institute of Technology (Wang lab 1737, Oka lab 1694-14). Mice were anesthetized with a mixture of ketamine (1 mg ml^{-1}) and xylazine (10 mg ml^{-1}) in isotonic saline, intraperitoneally injected at 10 μl/g body weight. Ketoprofen was subcutaneously administered at 5 μl/g body weight. Surgery was performed as previously described (*44*). The three-dimensional magnetic resonance imaging coordinate system was used as a reference for the injection site coordinates. Viral particles (titer, 3.5×10^{13} vg ml^{-1}) were injected using a microprocessor-controlled injection system (Nanoliter 2000, World Precision Instruments) at 100 nl min^{-1}. The coordinates for the motor cortex were as follows: anterior-posterior, +3100 μm; medial-lateral, +1100 μm; and ventral-dorsal, +650 μm (200 to 500 nl). Animals were placed in a clean cage after surgery, which was placed on a heating pad overnight, and then housed in the animal facility. Experiments were performed after at least 1 week of recovery.

Preparation of live brain slices

After decapitation, the mouse brain was extracted. Coronal slices of 900 μm in thickness were obtained using a vibratome (VT-1000s, Leica) in ice-cold sucrose-aCSF (artificial cerebrospinal fluid) solution (213 mM sucrose, 2.5 mM KCl, 1.2 mM NaH_2PO_4, 25 mM $NaHCO_3$, 10 mM glucose, 7 mM $MgSO_4$, and 1 mM $CaCl_2$). Slices were then incubated in normal aCSF (124 mM NaCl, 2.5 mM KCl, 1.2 mM NaH_2PO_4, 25 mM $NaHCO_3$, 10 mM glucose, 1 mM $MgSO_4$, and 2 mM $CaCl_2$, bubbled with 95% O_2/5% CO_2) at 34.5°C for 30 min and held at room temperature until use. For imaging, a slice was transferred into a chamber perfused with normal aCSF at room temperature.

Reproducibility

The experiments were not randomized. The investigators were not blinded to allocation during the experiments and outcome assessment. No sample size estimation was performed to ensure adequate power to detect a prespecified effect size.

SUPPLEMENTARY MATERIALS

Supplementary material for this article is available at http://advances.sciencemag.org/cgi/content/full/5/12/eaay1211/DC1

Note S1. Frequency shifting of the tagged photons.
Note S2. Mathematical description of GePGS-guided optical focusing inside scattering media.
Note S3. Minimizing the impact of the fast motions in scattering media.
Note S4. Curvature compensation and pixel matching.
Note S5. SNR of the averaged differential hologram.

Note S6. Filtering out the photons tagged by the GePGS from noise photons.
Fig. S1. Fluorescence spectra of DrBphP-PCM in the Pr state (OFF; red line) and after photoconversion to the Pfr state (ON; black line).
Fig. S2. Calculation of the binary amplitude map displayed on the DMD.
Fig. S3. DMD curvature compensation and pixel matching between the DMD and the camera.
Fig. S4. Relationship between the detected signals of tagged photons and the total cycle number.
Fig. S5. Fluorescence imaging of DrBphP-PCM in live neurons.
Fig. S6. Normalized intensity distribution of the optical foci inside the brain slices.
Movie S1. Principle of GePGS-guided optical focusing inside scattering media.
Movie S2. Time-reversed focusing inside mouse tumors in vivo.

View/request a protocol for this paper from *Bio-protocol*.

REFERENCES AND NOTES

1. V. Ntziachristos, Going deeper than microscopy: The optical imaging frontier in biology. *Nat. Methods* **7**, 603–614 (2010).
2. P. Lai, L. Wang, J. W. Tay, L. V. Wang, Photoacoustically guided wavefront shaping for enhanced optical focusing in scattering media. *Nat. Photonics* **9**, 126–132 (2015).
3. R. Sarma, A. G. Yamilov, S. Petrenko, Y. Bromberg, H. Cao, Control of energy density inside a disordered medium by coupling to open or closed channels. *Phys. Rev. Lett.* **117**, 086803 (2016).
4. S. M. Popoff, G. Lerosey, R. Carminati, M. Fink, A. C. Boccara, S. Gigan, Measuring the transmission matrix in optics: An approach to the study and control of light propagation in disordered media. *Phys. Rev. Lett.* **104**, 100601 (2010).
5. H. Yu, T. R. Hillman, W. Choi, J. O. Lee, M. S. Feld, R. R. Dasari, Y. Park, Measuring large optical transmission matrices of disordered media. *Phys. Rev. Lett.* **111**, 153902 (2013).
6. Z. Yaqoob, D. Psaltis, M. S. Feld, C. Yang, Optical phase conjugation for turbidity suppression in biological samples. *Nat. Photonics* **2**, 110–115 (2008).
7. J. Yang, Y. Shen, Y. Liu, A. S. Hemphill, L. V. Wang, Focusing light through scattering media by polarization modulation based generalized digital optical phase conjugation. *Appl. Phys. Lett.* **111**, 201108 (2017).
8. B. Judkewitz, Y. M. Wang, R. Horstmeyer, A. Mathy, C. Yang, Speckle-scale focusing in the diffusive regime with time reversal of variance-encoded light (TROVE). *Nat. Photonics* **7**, 300–305 (2013).
9. C. Ma, X. Xu, Y. Liu, L. V. Wang, Time-reversed adapted-perturbation (TRAP) optical focusing onto dynamic objects inside scattering media. *Nat. Photonics* **8**, 931–936 (2014).
10. J. Yang, J. Li, S. He, L. V. Wang, Angular-spectrum modeling of focusing light inside scattering media by optical phase conjugation. *Optica* **6**, 250–256 (2019).
11. R. Horstmeyer, H. Ruan, C. Yang, Guidestar-assisted wavefront-shaping methods for focusing light into biological tissue. *Nat. Photonics* **9**, 563–571 (2015).
12. X. Xu, H. Liu, L. V. Wang, Time-reversed ultrasonically encoded optical focusing into scattering media. *Nat. Photonics* **5**, 154–157 (2011).
13. K. Si, R. Fiolka, M. Cui, Fluorescence imaging beyond the ballistic regime by ultrasound-pulse-guided digital phase conjugation. *Nat. Photonics* **6**, 657–661 (2012).
14. H. Ruan, J. Brake, J. E. Robinson, Y. Liu, M. Jang, C. Xiao, C. Zhou, V. Gradinaru, C. Yang, Deep tissue optical focusing and optogenetic modulation with time-reversed ultrasonically encoded light. *Sci. Adv.* **3**, eaao5520 (2017).
15. I. M. Vellekoop, M. Cui, C. Yang, Digital optical phase conjugation of fluorescence in turbid tissue. *Appl. Phys. Lett.* **101**, 081108 (2012).
16. L. Kong, M. Cui, In vivo fluorescence microscopy via iterative multi-photon adaptive compensation technique. *Opt. Express* **22**, 23786–23794 (2014).
17. N. Ji, D. E. Milkie, E. Betzig, Adaptive optics via pupil segmentation for high-resolution imaging in biological tissues. *Nat. Methods* **7**, 141–147 (2010).
18. O. Katz, E. Small, Y. Guan, Y. Silberberg, Noninvasive nonlinear focusing and imaging through strongly scattering turbid layers. *Optica* **1**, 170–174 (2014).
19. E. H. Zhou, H. Ruan, C. Yang, B. Judkewitz, Focusing on moving targets through scattering samples. *Optica* **1**, 227–232 (2014).
20. F. Kong, R. H. Silverman, L. Liu, P. V. Chitnis, K. K. Lee, Y.-C. Chen, Photoacoustic-guided convergence of light through optically diffusive media. *Opt. Lett.* **36**, 2053–2055 (2011).
21. H. Ruan, T. Haber, Y. Liu, J. Brake, J. Kim, J. M. Berlin, C. Yang, Focusing light inside scattering media with magnetic-particle-guided wavefront shaping. *Optica* **4**, 1337–1343 (2017).
22. Z. Yu, J. Huangfu, F. Zhao, M. Xia, X. Wu, X. Niu, D. Li, P. Lai, D. Wang, Time-reversed magnetically controlled perturbation (TRMCP) optical focusing inside scattering media. *Sci. Rep.* **8**, 2927 (2018).
23. H. Ruan, M. Jang, C. Yang, Optical focusing inside scattering media with time-reversed ultrasound microbubble encoded light. *Nat. Commun.* **6**, 8968 (2015).
24. L. Li, thesis, California Institute of Technology (2019).
25. H. Takala, A. Björling, O. Berntsson, H. Lehtivuori, S. Niebling, M. Hoernke, I. Kosheleva, R. Henning, A. Menzel, J. A. Ihalainen, S. Westenhoff, Signal amplification and transduction in phytochrome photosensors. *Nature* **509**, 245–248 (2014).
26. J. Yao, A. A. Kaberniuk, L. Li, D. M. Shcherbakova, R. Zhang, L. Wang, G. Li, V. V. Verkhusha, L. V. Wang, Multiscale photoacoustic tomography using reversibly switchable bacterial phytochrome as a near-infrared photochromic probe. *Nat. Methods* **13**, 67–73 (2015).
27. L. Li, A. A. Shemetov, M. Baloban, P. Hu, L. Zhu, D. M. Shcherbakova, R. Zhang, J. Shi, J. Yao, L. V. Wang, V. V. Verkhusha, Small near-infrared photochromic protein for photoacoustic multi-contrast imaging and detection of protein interactions in vivo. *Nat. Commun.* **9**, 2734 (2018).
28. V. V. Lychagov, A. A. Shemetov, R. Jimenez, V. V. Verkhusha, Microfluidic system for in-flow reversible photoswitching of near-infrared fluorescent proteins. *Anal. Chem.* **88**, 11821–11829 (2016).
29. D. Akbulut, T. J. Huisman, E. G. van Putten, W. L. Vos, A. P. Mosk, Focusing light through random photonic media by binary amplitude modulation. *Opt. Express* **19**, 4017–4029 (2011).
30. D. Wang, E. H. Zhou, J. Brake, H. Ruan, M. Jang, C. Yang, Focusing through dynamic tissue with millisecond digital optical phase conjugation. *Optica* **2**, 728–735 (2015).
31. Y. Shen, Y. Liu, C. Ma, L. V. Wang, Focusing light through scattering media by full-polarization digital optical phase conjugation. *Opt. Lett.* **41**, 1130–1133 (2016).
32. J. Ge, M. Lan, B. Zhou, W. Liu, L. Guo, H. Wang, Q. Jia, G. Niu, X. Huang, H. Zhou, X. Meng, P. Wang, C.-S. Lee, W. Zhang, X. Han, A graphene quantum dot photodynamic therapy agent with high singlet oxygen generation. *Nat. Commun.* **5**, 4596 (2014).
33. N. M. Idris, M. K. Gnanasammandhan, J. Zhang, P. C. Ho, R. Mahendran, Y. Zhang, In vivo photodynamic therapy using upconversion nanoparticles as remote-controlled nanotransducers. *Nat. Med.* **18**, 1580–1585 (2012).
34. T.-W. Chen, T. J. Wardill, Y. Sun, S. R. Pulver, S. L. Renninger, A. Baohan, E. R. Schreiter, R. A. Kerr, M. B. Orger, V. Jayaraman, L. L. Looger, K. Svoboda, D. S. Kim, Ultrasensitive fluorescent proteins for imaging neuronal activity. *Nature* **499**, 295–300 (2013).
35. Y. Gong, C. Huang, J. Z. Li, B. F. Grewe, Y. Zhang, S. Eismann, M. J. Schnitzer, High-speed recording of neural spikes in awake mice and flies with a fluorescent voltage sensor. *Science* **350**, 1361–1366 (2015).
36. K. Deisseroth, Optogenetics. *Nat. Methods* **8**, 26–29 (2011).
37. E. S. Boyden, F. Zhang, E. Bamberg, G. Nagel, K. Deisseroth, Millisecond-timescale, genetically targeted optical control of neural activity. *Nat. Neurosci.* **8**, 1263–1268 (2005).
38. N. G. Horton, K. Wang, D. Kobat, C. G. Clark, F. W. Wise, C. B. Schaffer, C. Xu, In vivo three-photon microscopy of subcortical structures within an intact mouse brain. *Nat. Photonics* **7**, 205–209 (2013).
39. L. Li, L. Zhu, C. Ma, L. Lin, J. Yao, L. Wang, K. Maslov, R. Zhang, W. Chen, J. Shi, L. V. Wang, Single-impulse panoramic photoacoustic computed tomography of small-animal whole-body dynamics at high spatiotemporal resolution. *Nat. Biomed. Eng.* **1**, 0071 (2017).
40. A. V. Leopold, K. G. Chernov, A. A. Shemetov, V. V. Verkhusha, Neurotrophin receptor tyrosine kinases regulated with near-infrared light. *Nat. Commun.* **10**, 1129 (2019).
41. R. C. Challis, S. R. Kumar, K. Y. Chan, C. Challis, K. Beadle, M. J. Jang, H. M. Kim, P. S. Rajendran, J. D. Tompkins, K. Shivkumar, B. E. Deverman, V. Gradinaru, Systemic AAV vectors for widespread and targeted gene delivery in rodents. *Nat. Protoc.* **14**, 379–414 (2019).
42. P. Lai, X. Xu, L. V. Wang, Dependence of optical scattering from Intralipid in gelatin-gel based tissue-mimicking phantoms on mixing temperature and time. *J. Biomed. Opt.* **19**, 35002 (2014).
43. Y. Liu, P. Lai, C. Ma, X. Xu, A. A. Grabar, L. V. Wang, Optical focusing deep inside dynamic scattering media with near-infrared time-reversed ultrasonically encoded (TRUE) light. *Nat. Commun.* **6**, 5904 (2015).
44. Y. Oka, M. Ye, C. S. Zuker, Thirst driving and suppressing signals encoded by distinct neural populations in the brain. *Nature* **520**, 349–352 (2015).

Acknowledgments: We thank J. Ihalainen (University of Jyväskylä, Finland) for the DrBphP gene, M. Monakhov for the isolation of neurons and help with their imaging and H. Ruan for insightful discussions on the work. **Funding:** This work was supported by NIH grants GM122567 and NS103573 (both to V.V.V.) and EB016986 (NIH Director's Pioneer Award), CA186567 (NIH Director's Transformative Research Award), NS090579, and NS099717 (all to L.V.W.). **Author contributions:** L.L., J.Y., Y.L., and L.V.W. conceived the study. L.L. and J.Y. designed the experiments. J.Y. constructed the DOPC system. J.Y., L.L., Y.L., Y.S., and J.L. performed the DOPC experiments. A.A.S. and V.V.V. constructed the plasmids, characterized the purified proteins, established the stable cell lines, and prepared the AAVs. L.L. and A.A.S. cultured the mammalian cells. S.L., Y.Z., and Y.O. performed the AAV transfection in vivo and prepared the brain slices. J.Y. and L.L. analyzed the data. L.V.W. supervised the study. J.Y., L.L., A.A.S., V.V.V., and L.V.W. wrote the manuscript. All authors reviewed the manuscript. **Competing interests:** L.V.W. has a financial interest in Microphotoacoustics Inc., CalPACT LLC, and Union Photoacoustic Technologies Ltd., which, however, did not support this work. The other authors declare no competing financial interests. **Data and materials availability:** All data needed to evaluate the conclusions in the paper are present in the paper and/or the Supplementary Materials. Additional data related to this paper may be requested from the authors.

Submitted 23 May 2019
Accepted 9 October 2019
Published 11 December 2019
10.1126/sciadv.aay1211

Citation: J. Yang, L. Li, A. A. Shemetov, S. Lee, Y. Zhao, Y. Liu, Y. Shen, J. Li, Y. Oka, V. V. Verkhusha, L. V. Wang, Focusing light inside live tissue using reversibly switchable bacterial phytochrome as a genetically encoded photochromic guide star. *Sci. Adv.* **5**, eaay1211 (2019).